PAPER

Evidence for a core–shell configuration in Tb-doped KY_3F_{10} nanoparticles using synchrotron x-ray line profile and pair distribution function analyses

To cite this article: R U Ichikawa *et al* 2018 *Mater. Res. Express* **5** 015006

Materials Research Express

PAPER

Evidence for a core–shell configuration in Tb-doped KY_3F_{10} nanoparticles using synchrotron x-ray line profile and pair distribution function analyses

RECEIVED
9 November 2017

REVISED
5 December 2017

ACCEPTED FOR PUBLICATION
11 December 2017

PUBLISHED
4 January 2018

R U Ichikawa[1], H S M D Linhares[2], I Peral[3,4], S L Baldochi[1], I M Ranieri[1], X Turrillas[5,6] and L G Martinez[1]

[1] Instituto de Pesquisas Energéticas e Nucleares, IPEN-CNEN/SP, Butantã, São Paulo, SP 05508-900, Brazil
[2] Universidade Federal Fluminense, UFF/INFES, Instituto do Noroeste Fluminense de Educação Superior, Santo Antônio de Pádua, Rio de Janeiro, RJ 28470-000, Brazil
[3] Université du Luxembourg, Faculté des Sciences, de la Technologie et de la Communication, 162 A, Avenue de la Faïencerie, L-1511Esch-sur-Alzette, Luxembourg
[4] Luxembourg Institute of Science and Technology, Materials Research and Technology Department, Belval Innovation Campus 5, Avenue des Hauts-Fourneaux, L-4362 Esch-sur-Alzette, Luxembourg
[5] Institut de Ciència de Materials de Barcelona, ICMAB/CSIC, Department of Crystallography, Campus de la UAB, Cerdanyola del Vallès, E-08193 Barcelona, Spain
[6] ALBA Synchrotron, Carrer de la Llum 2-26, Cerdanyola del Vallès, E-08290 Barcelona, Spain

E-mail: ichikawa@usp.br

Keywords: x-ray diffraction, x-ray line profile analysis, pair distribution function analysis, KY_3F_{10} nanoparticles, core–shell configuration

Abstract

The microstructure of Tb-doped KY_3F_{10} nanoparticles synthesized by coprecipitation was analysed using x-ray synchrotron diffraction data. Size-strain analysis was performed by means of x-ray line profile (XLPA) methods such as Warren–Averbach and whole powder pattern modelling. Additionally, the structural coherence of the sample was accessed using pair distribution function analysis, supporting the XLPA results. The combination of all methods revealed that the nanoparticles exhibit a more ordered core and a less ordered surface comprising a core–shell configuration.

1. Introduction

Lanthanide-doped upconversion nanoparticles present very interesting optical properties such as high photochemical stability, sharp emission bandwidths, long fluorescent lifespan, multiple emission bands among others [1, 2]. A very interesting type of upconversion nanomaterial are rare-earth doped KY_3F_{10} nanoparticles, that exhibit interesting luminescence properties, which can be tuned by varying its mean crystallite size [3, 4]. It was seen that when the crystallites become progressively larger, there is an ion redistribution within the particle with a gradient towards its surface. Specifically, Tb-doped KY_3F_{10} nanoparticles are very interesting for radiation dosimetry applications [5]. So, a detailed size-strain analysis is very important to fully understand Tb-doped KY_3F_{10} properties, especially to help elucidate the microstructure role in the luminescence dynamics.

In this work, mean crystallite size and size distribution were determined using x-ray line profile analysis (XLPA) such as Warren–Averbach (WA) [6] and whole powder pattern modelling (WPPM) [7]. WA method is still the most unbiased method to probe the microstructure using x-ray diffraction data since it does not assume any function to model the diffraction peaks. Mean crystallite size and microstrain can be obtained by Fourier transforming the diffraction peaks. Besides, WPPM is a state-of-the-art method to also obtain size-strain information of nanocrystalline specimens by modelling the whole diffraction pattern assuming spherical or cubic shaped crystallites. Moreover, with WPPM the microstrain can be easily accessed by refinable parameters computed by PM2K [7], the software used to model the diffraction pattern using WPPM. In this sense, WA and WPPM can be used simultaneously and complementarily to fully describe the nanoparticle microstructure. Additionally, the structural coherence of the system was analysed by pair distribution function (PDF) analysis to support the results obtained by XLPA. The combination of all these methods revealed that the Tb-doped KY_3F_{10}

nanoparticles can be described by a core–shell configuration, with a more ordered core and a less ordered and strained surface.

2. Experimental

Tb-doped KY_3F_{10} nanoparticles were synthesized using coprecipitation by dissolving Y_2O_3 and Tb_2O_3 (Aldrich 99.9%) in HCl and then adding an aqueous solution of KF (Merck 99%). For a detailed description of the synthesis route the reader can consult [8].

Transmission electron microscopy (TEM) images were obtained using a JEOL model JEM-200C microscope with an acceleration voltage of 200 kV. X-ray synchrotron diffraction measurements were carried out in the materials science powder diffraction beamline (MSPD) [9] at ALBA synchrotron light source. MSPD has a superconducting wiggler, operating under a magnetic field of 2 T, as photon source capable of achieving high energies. In fact, it operates within a range of 8–50 keV; such range adequately covers the desirable scope of this study. For the work here presented, the diffraction data were collected with 30 keV photons at room temperature. The specimens were introduced in 0.8 mm diameter Lindemann capillary tubes and kept rotating during the acquisition. The detector system used was a Mythen II of six modules, covering an angular domain of 40°. The setup provided high counting statistics that also allowed the proper application of XLPA and PDF analyses.

3. Methods

3.1. WA method

In the WA method [6] the x-ray diffraction profile can be represented as a Fourier series in the reciprocal space. Its Fourier coefficient ($A(L)$) is the product of two terms, one dependent on the column length of unit cells, hence related to the crystallite size ($A^S(L)$) and another related to the deformation in the crystal lattice ($A^D(L)$), which depends on d^{-1}, where d is the interplanar distance of the analysed material, and therefore is a function of the reflection order of the profile considered. The mean crystallite size can be determined from a plot of $A^S(L)$ versus L, which provides the area-weighted mean crystallite size $\langle L\rangle_A$ [6, 10]. To calculate the crystallite size distribution, the volume-weighted mean crystallite size $\langle L\rangle_V$ is needed. $\langle L\rangle_V$ can be obtained from [11]:

$$\langle L\rangle_V = 2\int_{-\infty}^{+\infty} A^S(L)\,\mathrm{d}L. \tag{1}$$

Both, $\langle L\rangle_A$ and $\langle L\rangle_V$ can be used to calculate the crystallite size distribution ($g(L)$), which in a powdered sample is influenced by several factors, including the condition of synthesis, heat treatments among other factors. Many studies [12–15] reported that the lognormal distribution is the most appropriate to describe the crystallite size distribution and was used in this work.

3.2. Whole powder pattern modelling (WPPM)

WPPM [7] describes the line profiles through microstructural models without using analytical functions. Basically, WPPM considers the Fourier transform (FT) of the diffraction peaks, so microstructural properties such as mean crystallite size and microstrain can be combined in one term by multiplying the FT's of each contribution present in the sample. This is very useful since terms can be easily added to the modelling. In this work, the modelling was performed using PM2K v.3 software [7]. Mean crystallite size and size distribution were modelled considering spherical shaped domains. The microstrain was analyses using the model proposed by Scardi and Leonardi [16, 17], which accounts for strain anisotropy. The Warren plots [6] can be obtained from the model, which permits the analysis of the local atomic displacement, also referred as root mean square displacement (RMSD).

4. Results and discussion

The Tb-doped KY_3F_{10} crystallites can be seen in the TEM presented in figure 1. Spherical shaped crystallites of approximately 9 nm can be appreciated. Also, interplanar spacings of approximately 5.779 and 3.337 Å can be observed in the inset of figure 1, which corresponds to the {002} and {222} family planes of the cubic structure with an angle of 55° between the planes.

Then, to perform the XLPA three sets from available parallel crystallographic directions in the x-ray measured profile were chosen: [111]-[222], [002]-[044] and [022]-[044]. These reflections provide a good overview of the crystallite size in various crystallographic directions. However, the reflections [002]-[111], [222]-[004], [044]-[531]- [442] are partially overlapped (see figure 2). Indeed, Bragg peaks overlapping is the main

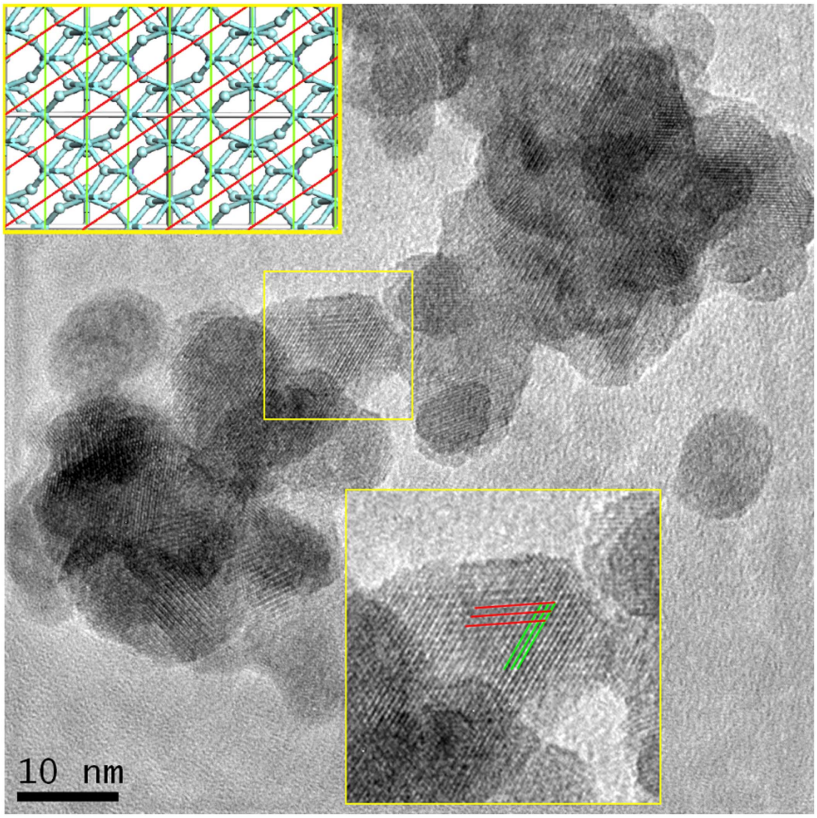

Figure 1. Transmission electron microscopy for the Tb-doped nanoparticles, where spherical shaped crystallites can be seen. The bottom inset, shows a zoomed in area with the family planes {002} (red lines) and {222} (green lines) of the cubic structure. The upper inset shows an illustration of the view along [110] zone axis direction, the same showed in the zoomed in area.

problem when applying WA method. To overcome such a situation, they were deconvolved using a Levenberg and Marquardt algorithm, which is ideal when nonlinear functions are fitted. In this case a Voigt function was selected and the results of the deconvolutions can be seen in figure 2.

After the deconvolution, WA method was applied using a procedure described in previous works [18, 19]. For the instrumental contribution correction, Si 640d SRM from NIST was used. The results are shown in table 1. It is possible to conclude that the crystallite sizes estimated along the various directions are comparable and not too disperse, indicating an isotropic crystallite shape, as expected from the spherical crystallites from figure 1. In addition, the analysis revealed low values for the root mean square strain (RMSS); moreover for the [111]-[222] and [022]-[044] crystallographic directions, yielded negative values for MSS, that statistically can be considered negligible [20].

To complement the results from WA method, WPPM was performed. For the modelling, spherical shaped crystallites were used and again Si 640d SRM was used to correct the x-ray profile from instrumental contributions. Cell parameter and background was fitted (using a Chebyshev polynomial of 6th order). Firstly, one cubic phase ($Fm\bar{3}m$ S. G., No. 225) was used to describe the structure. However, as it can be seen in figure 3(a), the calculated model is slightly scant to describe the experimental data, especially in the 6.5°–9.0° and 10.5°–14.0° regions, where the intensities are not well fitted, for this modelling a final $R_{wp} = 7.1\%$ was achieved.

In this work, the R_{wp} factor was considered to evaluate the model agreement, since is the most used discrepancy term when refinements such as Rietveld or WPPM are applied. R_{wp} stands for weighted profile R-factor determined by the square root of the difference between the calculated model and the experimental data. This difference is scaled taking into account the weighted intensities of the profile [21].

Besides that, the mean crystallite size value obtained ($\langle L \rangle_{WPPM} = 4.2$ nm) is far from the ones observed in the TEM image and the ones obtained from WA method. In various works [22–25] it is reported that nanoparticles present in its surface a strained region, which is mainly caused by the high energy concentration of defects that arises from its large superficial area. Considering that this surface strained region is not so different from the inner part and it is less ordered, its contribution to the x-ray profile will be mainly located underneath the peaks of the main inner phase.

Thus, the modelling was performed again using two phases, considering that the nanoparticle has a more ordered inner structure and a strained surface, like a core–shell system. As can be seen in figure 3(b), the

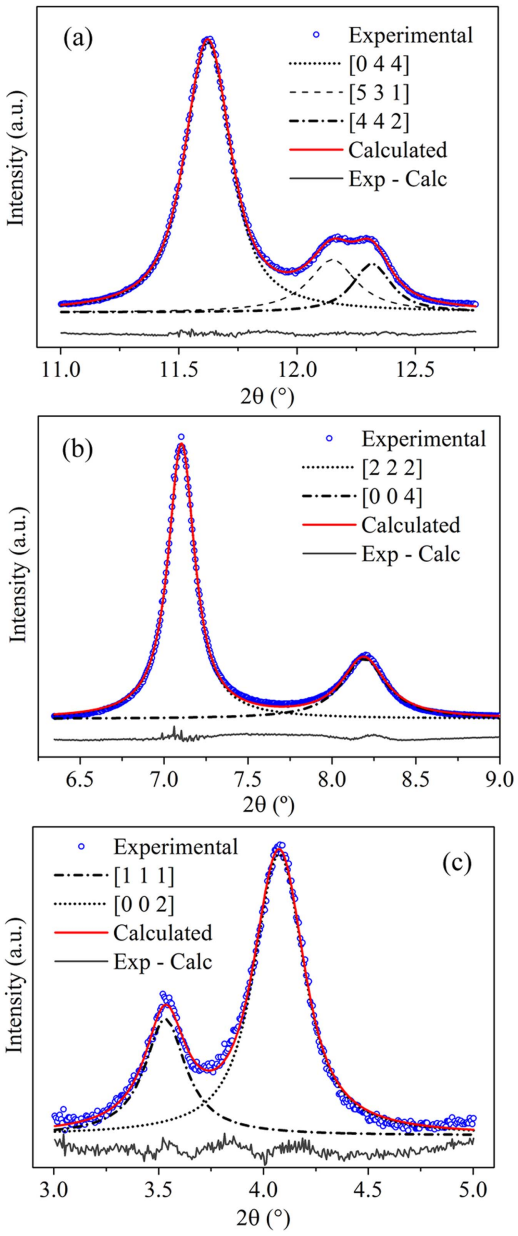

Figure 2. Experimental (blue dots) and calculated (red line) synchrotron powder diffraction peaks for the application of the WA method. Below the peaks (grey line) is the difference between the calculated and experimental data.

Table 1. Area-weighted $\langle L \rangle_A$, volume-weighted $\langle L \rangle_V$, root mean square strain, mean crystallite size and standard deviation (σ) of the distribution. The subscripts WA and WPPM stands for the mean size of the distribution obtained by Warren–Averbach and whole powder pattern modelling, respectively. Size related values expressed in nm.

	Warren–Averbach			Distribution		WPPM	
Direction	$\langle L \rangle_A$	$\langle L \rangle_V$	RMSS	$\langle L \rangle_{WA}$	σ	$\langle L \rangle_{WPPM}$	σ
[111]-[222]	7.0(1)	9.1(3)	0[a]	7.9(2)	3.1(1)	9.0(4)	3.5(1)
[002]-[004]	6.5(2)	7.7(2)	2.8(5)	8.8(1)	2.0(2)		
[022]-[044]	7.6(1)	8.8(2)	0[a]	10.8(2)	1.8(1)		

[a] Mean square strain was a small negative number. RMSS was set to zero [20].

modelling improved with a final $R_{wp} = 4.4\%$ and cell parameter $a = 11.543\,94(7)$ Å. The main improvement can be seen for the peak intensities, as stated previously, in the 6.5°–9.0° and 10.5°–14.0° regions, as a consequence of the second phase addition. Besides that, the value for the mean crystallite size (see table 1) is

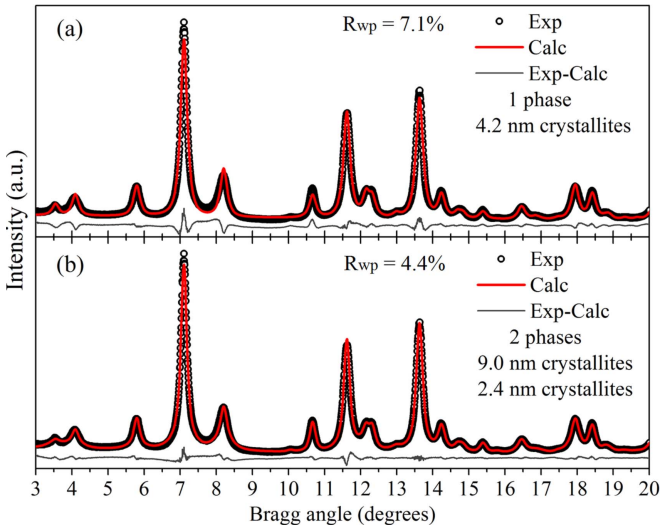

Figure 3. Whole powder pattern modelling applied to x-ray synchrotron diffraction data of Tb-doped KY_3F_{10} nanoparticles. Considering (a) one phase and (b) two phases.

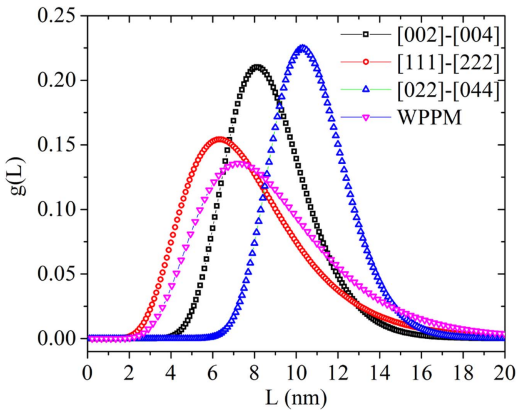

Figure 4. Crystallite size distribution determined using Warren–Averbach for three directions and whole powder pattern modelling.

more compatible with TEM image and WA method. This result is easier to visualize by the distribution curves in figure 4. The distribution calculated with the core–shell model in WPPM yields $\langle L\rangle_{\mathrm{WPPM}} = 9.0(4)$ nm. Taking the average for the mean values of $\langle L\rangle_{\mathrm{WA}}$ in the three directions, it gives $\overline{\langle L\rangle_{\mathrm{WA}}} = 9.2$ nm. For the shell region, a mean crystallite size value of 2.4 nm was found, which is plausible since the shell is expected to be less ordered and smaller when compared to the core.

Also, the microstrain for the core was analysed by the Warren plots, which can be seen in figure 5. The plot gives the RMSD between two atoms separated by a distance L inside the crystallite. This type of analysis is very useful since it permits the visualization of the strain behaviour in all directions as a function of the distance L. The monotonic behaviour of the curves in the Warren-plots for all directions, i.e. a gradual increase for RMSD values, reveal that low microstrain in present, which is a typical behaviour for a more ordered region.

The microstrain was not analysed for the shell since it comprises a very small region (~2.4 nm), so its contribution to the x-ray diffraction profile result in very broad peaks (see figure 6) and the application of the strain model in such broad profile would not provide reliable results. However the core–shell configuration proposed in this work can explain a local distortion detected in a previous study [8]. The local structure of the same batch of nanoparticles was analysed in detail using PDF analysis. It was found that small tetragonal domains are within the structure. As could be seen from the Warren-plots, the core region presents a monotonic and well-defined increase in the RMSD, implying that in the core those tetragonal domains cannot be present, since no major distortion was seen. The only possible explanation is that the shell of the nanoparticle concentrates such tetragonal nanodomains. In other words, the nanoparticle has a more ordered cubic

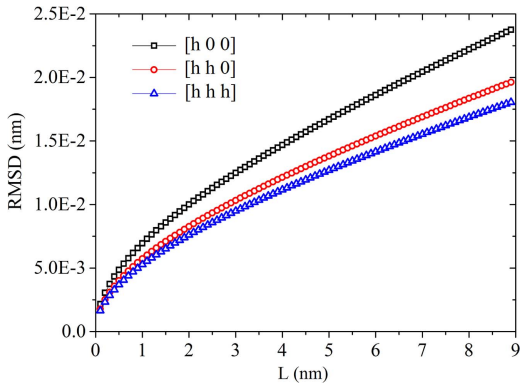

Figure 5. Warren plots for the Tb-doped KY_3F_{10} nanoparticles in all crystallographic directions.

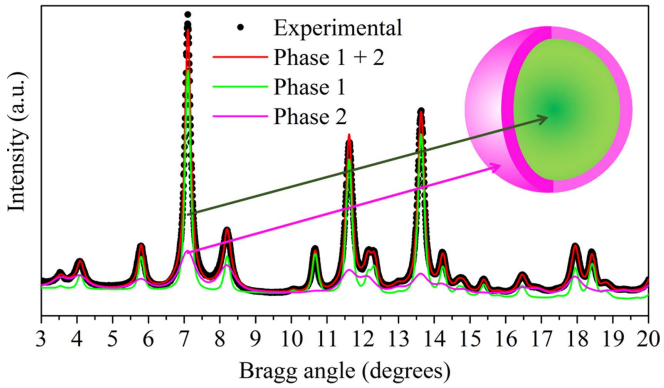

Figure 6. WPPM modelling considering two phases: a more ordered one forming the core and a less ordered located in the shell. The inset shows the core–shell system and the contribution of each phase.

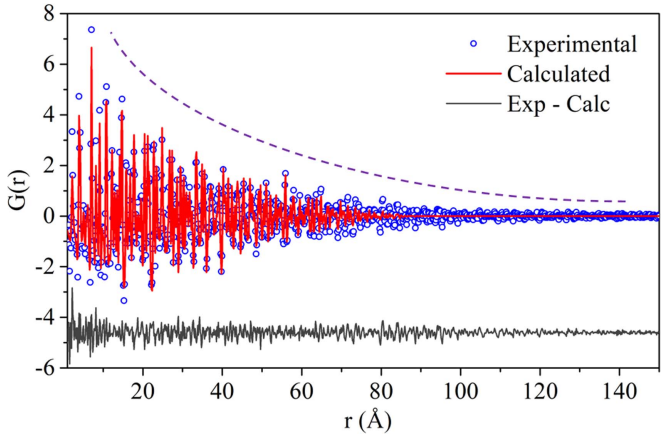

Figure 7. X-ray synchrotron PDF data refinement for the Tb-doped nanoparticles. The dashed line highlights the PDF attenuation due to its finite nanometer size.

crystalline inner structure and near the surface, the structure becomes strained and less ordered resulting in the tetragonal nanodomains observed by PDF analysis.

Lastly, the structural coherence was analysed from PDF data. This is possible considering the dampening of the PDF signal for high-r values (see figure 7). The PDF $G(r)$ attenuation corresponds to the decrease of the numbers of atoms pairs inside the nanostructure. The software used to model the PDF data was PDFgui [26] that allows the estimation of crystallite size, assuming a spherical shape. It is worth to mention that the use of PDF to estimate the crystallite size was recently performed by Gamez-Mendoza *et al* [27], where it was demonstrated

that reliable results regarding crystallite size and its distribution can be obtained with PDF data. So, first the refinement was performed in a similar way for Si 640d SRM PDF data to determine the dampening due to instrumental resolution. In PDFgui, the parameter 'spdiameter' accounts for the effect of the finite size of the nanoparticle giving an estimation for its diameter. In figure 7, the PDF refinement can be seen. The attenuation of $G(r)$ due to the finite domain size is clearly present. The value found for the nanoparticle diameter was 9.4(5) nm, in agreement with all XLPA methods applied previously.

5. Conclusions

In this work, XLPA and PDF analyses were used to probe the microstructure of Tb-doped KY_3F_{10} nanoparticles. A core–shell configuration was proposed to explain the results from XLPA methods. The results indicated that the nanoparticles have mean crystallite size of approximately 9 nm and low microstrain in the core, but present a strained surface. According to the two-phase model, the strained surface can be explained as composed by small tetragonal nanodomains, detected as a local structure in a previous work [8]. Lastly, PDF was used to probe the structural coherence and it was seen that PDF peaks fade away at approximately 9 nm, in accordance with XLPA methods.

Acknowledgments

RUI acknowledges CAPES and CNPq (No. 206983/2014-0) for the scholarships. The XRD experiment was performed at MSPD beamline at ALBA Synchrotron with the collaboration of ALBA staff. Professor Paolo Scardi from University of Trento is acknowledged for the discussions and for providing PM2K v.3 software. HMSDL and SLB acknowledges CNPq for financial support (Photonics National Institute for Science and Technology). IP is supported by the National Research Fund of Luxembourg (Grant No FNR-Inter2015/LRSF). XT would like to acknowledge the financial support from the Spanish MINECO projects MAT2015-67593-P and BIA2014–57658-C2-1-R.

ORCID iDs

R U Ichikawa https://orcid.org/0000-0002-7661-9999

References

[1] Wang F, Han Y, Lim C S, Lu Y, Wang J, Xu J, Chen H, Zhang C, Hong M and Liu X 2010 *Nature* **463** 1061–5
[2] Chen C, Chunguang L and Shi Z 2016 *Adv. Sci.* **3** 1600029
[3] Gomes L, Linhares H M S M D, Ichikawa R U, Martinez L G and Ranieri I M 2015 *J. Lumin.* **157** 285–92
[4] Gomes L, Linhares H M S M D, Ichikawa R U, Martinez L G and Baldochi S L 2016 *Opt. Mater.* **54** 57–66
[5] Linhares H M S M D 2014 Síntese de nanocristais de KY3F10 pelo método de co-precipitação visando aplicações ópticas *PhD thesis* Universidade de São Paulo, São Paulo, Brazil
[6] Warren B E and Averbach B L 1950 *J. Appl. Phys.* **21** 595–9
[7] Scardi P 2008 Microstructural properties: lattice defects and domain size effects ed R E Dinnebier and S J L Billinge *Powder Diffraction: Theory and Practice* (Cambridge: The Royal Society of Chemistry) ch 13
[8] Ichikawa R U, Linhares H M S M D, Peral I, Baldochi S L, Ranieri I M, Turrillas X and Martinez L G 2017 *ACS Omega* **2** 5128–36
[9] Fauth F, Peral I, Popescu C and Knapp M 2013 *Powder Diffr.* **V28** S360–70
[10] de Keijser T, Mittemeijer E J and Rozendaal H C F 1983 *J. Appl. Cryst.* **16** 309–16
[11] Krill C E and Birringer R *Phil. Mag.* A **77** 621–40
[12] Balzar D 1999 Voigt-function model in diffraction line-broadening analysis ed H J Bunge and J Fiala *Microstructure Analysis from Diffraction, International Union of Crystallography* (Oxford: Oxford University Press)
[13] Langford J I 2000 *J. Appl. Cryst.* **33** 964–74
[14] Popa N C and Balzar D 2002 *J. Appl. Cryst.* **35** 338–46
[15] Ida T, Shimazaki S, Hibino H and Toraya H 2002 *J. Appl. Cryst.* **35** 1107–15
[16] Scardi P, Leonardi A, Gelisio L, Suchomel M R, Sneed B T, Sheehan M K and Tsung C-K 2015 *Phys. Rev.* B **91** 155414
[17] Leonardi A and Scardi P 2016 *Metall. Mater. Trans.* A **47** 5722–32
[18] Ichikawa R U 2013 Aplicações do método de Warren–Averbach de análise de perfis de difração *Master's Dissertation* [São Paulo, Brazil]: University of São Paulo
[19] Ichikawa R U, Martinez L G, Imakuma K and Turrillas X 2014 Development of a methodology for the application of the Warren–Averbach method *Encontro Científico de Física Aplicada [= Blucher Physics Proc., n.1, v.1]* (São Paulo: Blucher)
[20] Balzar D *et al* 2004 *J. Appl. Cryst.* **37** 911–24
[21] Toby B H 2006 *Powder Diffr.* **21** 67–70
[22] Zhou X-D and Huebner W 2001 *Appl. Phys. Lett.* **79** 3512–4
[23] Gilbert B, Huang F, Zhang H, Waychunas G A and Banfield J F 2004 *Science* **305** 651–4
[24] Leoni M and Scardi P 2004 Grain surface relaxation effects in powder diffraction ed P Scardi and E J Mittemeijer *Diffraction Analysis of the Microstructure of Materials.* (Berlin: Springer)

[25] Masadeh A S 2016 *J. Exp. Nanosci.* **11** 951–74
[26] Farrow C L, Juhas P, Liu J W, Bryndin D, Božin E S, Bloch J, Proffen T and Billinge S J 2007 *J. Phys.: Condens. Matter* **19** 335219
[27] Gamez-Mendoza L, Terban M W, Billinge S L and Martinez-Inesta M 2017 *J. Appl. Cryst.* **50** 689–700